

Visibility-Inspired Models of Touch Sensors for Navigation

Kshitij Tiwari¹, Basak Sakcak¹, Prasanna Routray², Manivannan M.², and Steven M. LaValle¹

Abstract—This paper introduces mathematical models of touch sensors for mobile robotics based on visibility. Serving a purpose similar to the pinhole camera model for computer vision, the introduced models are expected to provide a useful, idealized characterization of task-relevant information that can be inferred from their outputs or observations. This allows direct comparisons to be made between traditional depth sensors, highlighting cases in which touch sensing may be interchangeable with time of flight or vision sensors, and characterizing unique advantages provided by touch sensing. The models include contact detection, compression, load bearing, and deflection. The results could serve as a basic building block for innovative touch sensor designs for mobile robot sensor fusion systems.

I. INTRODUCTION

Touch sensor designs have evolved over the past four decades yet the touch modality is not as deeply explored as vision and auditory. The existing touch sensors are often inspired by touch receptors and are aimed at robotic and industrial applications which typically require human-like prehensile manipulation capabilities for the robots to work safely around humans. In this work, look further to explore the possibility of using the touch modality for navigation with mobile robots. In nature, mammals (like rats, shrews, pinnipeds etc.) and fishes use the touch modality for navigation utilizing pre- and post-contact touch feedback.

For navigation in unknown and unstructured environments researchers typically resort to distal sensors such as cameras and Lidars. The utility of such sensors may seem limiting when it comes to cases where a robot needs to navigate in dimly lit environments. Similarly, soft terrains present wheel slippage and sinkage challenges for ground robots and the space exploration community can benefit from such solutions [2]. Although vision-based solutions such as [3] exist, these approaches are often prone to failure under sudden illumination changes and dust. Similarly, when inspecting underwater mines using an autonomous marine vehicle, the murky and rough waters may even harm the optical sensors [4]. Few researchers have started looking into potential use cases of vibrissae-enabled robots [5]. Rodents use their vibrissae, a form of touch sensor, to detect both tactile and kinesthetic features [6]. Although tactile features

help infer the surface profile through textural perception [1], kinesthetic features are perceived through proprioception [7], which can be thought of as self-localization.

In this work, we investigate the utility of touch sensors mounted on a mobile robot for proprioception. Some touch sensors provide very limited information such as the bumper sensors (see Figs. 1a, 1b) whereas others could capture a lot more information about the objects such as their surface profile. As surface profile provides a qualitative idea about the environment, profile sensing with touch sensors can augment the path planning capability for mobile robots. We consider two types of touch sensors- *rigid* and *compliant* where compliance is limited to their ability to compress (change its volume under applied transverse load, as in Figs. 1c, 1d) or bend (similar to the vibrissae shown in Fig. 1e). Compressible touch sensors can be used for motion planning for collision resilient robots as was shown in [8] and hence, we consider compressibility as a desirable form of compliance for touch sensors. Also, we are interested in contrasting the quality of information between actuated and unactuated touch sensors. For instance, in [9], an actuated probe (rigid link) was used for terrain identification to guide the otherwise blind robot through an environment while avoiding dangerous patches. In [10], the researchers showed how actuation directly impacts object localization. They considered two variants of a whisker-like touch sensor array- one actuated like the motile macrovibrissae and the other static like the immotile microvibrissae. They showed that the static touch sensor had relatively poor object localization accuracy, and in this work we analyze such claims in terms of preimages.

To contrast various touch sensors, we resort to *virtual sensor models* from [11]. The aim here is to compare the sensors in terms of their preimages, and develop mathematical models independent of their physical realization. Serving a purpose similar to the pinhole camera model for computer vision, the introduced models are expected to provide a useful, idealized characterization of task-relevant information that can be inferred from their outputs or observations. This could elucidate various aspects of touch sensors to increase the task success rate when deploying mobile robots in unstructured environments.

II. VIRTUAL TOUCH SENSOR MODELS

There is a wide spectrum of touch sensors available in the literature, some of which were discussed above. But the question remains, given any two touch sensors, how does one know which is superior compared to the other? A coarse elimination is possible given some prior

¹Center of Ubiquitous Computing, Faculty of Information Technology and Electrical Engineering, University of Oulu, Oulu, Finland, firstname.lastname@oulu.fi

²Touch Lab, Center for Virtual Reality and Haptics, Indian Institute of Technology Madras, India

This work was supported by a European Research Council Advanced Grant (ERC AdG, ILLUSIVE: Foundations of Perception Engineering, 101020977), Academy of Finland (projects PERCEPT 322637, CHiMP 342556), and Business Finland (project HUMOR 3656/31/2019).



Fig. 1: Various types of touch sensors. 1a and 1b are common contact detectors; 1c and 1d are typical compressible touch sensors (Images from e-ptnk.co.kr/eng/pogo-pin/ and hoffmann-krippner.com/types-of-lvdt/, respectively). LVDT stands for Linear Variable Differential Transducer; 1e shows macro- and microvibrissae in rats [1].

knowledge of the downstream task, but then given a family of sensors suited to the task, how does one narrow down to the optimal sensor? Every transducer and design has strengths and weaknesses making it difficult to do a fair comparison. To facilitate this discussion, here we discuss the concept of *virtual sensors* from [11]. A *virtual sensor* is a mathematical abstraction of the sensor, different from the models that explain its physics, and independent of its physical realization thereby allowing a fair comparison. In what follows, we will first describe the concept of sensor mapping followed by formally defining the state spaces. Then, we present various virtual touch sensors followed by a discussion on compositions of such models and their comparison with conventional visibility-based sensors.

A. Sensor Mapping

Even though the mathematical model that explains the physics of a sensor varies with its design we can define a virtual sensor [11] as a mapping,

$$h : X \rightarrow Y, \quad (1)$$

from the robot's state space X to the observation space Y . The state space X refers to the set of all the states that the robot can be in and the observation space Y is the set of all possible observations (measurements) that a sensor can make. In the following, we will refer to h as the sensor mapping. In order to lighten the notation, in the following sections, when describing some sensors, we will use $h(x; m)$ to describe a sensor mapping for which m are the parameters.

Typically a sensor mapping is not bijective; whereas each $x \in X$ maps to a single $y \in Y$, multiple states can give out the same observation. Therefore, in the general case, the sensor mapping is not invertible and the preimage of y under h , written as $h^{-1}(y)$, is defined as the set,

$$h^{-1}(y) = \{x \in X \mid y = h(x)\}. \quad (2)$$

Note that if the sensor mapping is bijective, then Eq. (2) corresponds to the inverse of the function h . As h is defined over the state space X , the subsets of X corresponding to the preimages of h form a partition of X denoted by $\Pi(h)$.

Consider two sensors, h_1 and h_2 , defined over the same fixed state space X that has different observation spaces Y_1 and Y_2 . If the partition $\Pi(h_1)$ is a refinement of $\Pi(h_2)$ then h_1 can simulate h_2 which means that there exists a function

$g : Y_1 \rightarrow Y_2$ such that $h_2(x) = g(h_1(x))$, written as $h_2 = g \circ h_1$ [11]. Two sensors are equivalent, denoted by $h_1 \cong h_2$, if the partition induced by the sensors, $\Pi(h_1)$ and $\Pi(h_2)$, respectively, satisfies $\Pi(h_1) = \Pi(h_2)$. If two sensors are equivalent they can simulate each other.

B. State Space

We consider a mobile robot moving in a 2D planar environment W which is the closure of the open set that is piecewise diffeomorphic to a finite disjoint union of circles. The boundary of W is denoted as ∂W . The robot is equipped with a touch sensor which can be seen as a link attached to the robot base whose characteristics vary across different models. However, the discussion in this work is limited to touch sensors that are either rigid or compliant that too either compressible or bendable.

We will refer to three coordinate frames and the corresponding homogeneous transformations between them as shown in Fig 2a. We express the configurations of the touch sensor and the robot as q_s and q_r , respectively. Then, $(q_x, q_y) \in W$ and $q_\theta \in S^1$ are the position and the orientation of the robot with respect to an absolute reference frame (world frame), respectively. The robot configuration q_r is defined by $q_r = (q_x, q_y, q_\theta)$. The world frame corresponds to an absolute reference frame with respect to which the robot configuration is defined. The robot frame and the sensor frame are the reference frames attached to the robot and the touch sensor, respectively. The homogeneous transform between the robot frame and the world frame is given by $T_{rw}(q_r)$ and varies with the configuration of the robot q_r . As for the touch sensor in its nominal form, it is aligned with the x-axis of the sensor frame (see Figs. 2b and c) which will be referred as the sensor axis from hereon. For unactuated touch sensors, the sensor frame is fixed with respect to the robot frame and T_{sr} is the homogeneous transform between two coordinate frames. To simplify the notation, we will assume that the robot frame and the sensor frame coincide for unactuated touch sensors, such that T_{sr} is an identity matrix. In cases where the touch sensor is actuated, the homogeneous transform between the sensor and robot frame is given by $T_{sr}(\psi)$ in which $\psi \in S^1$ is the amount of rotation of the sensor frame with respect to the robot frame.

We now define the configurations of compliant touch sensors. Compressible touch sensors can compress along the sensor axis, similar to a linear spring or a link attached to a prismatic joint (like Figs. 1c and 1d). The sensor

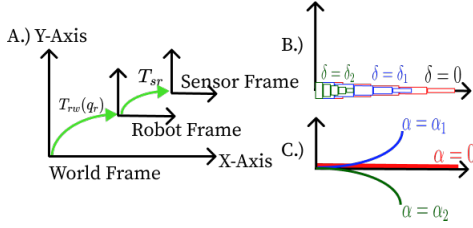


Fig. 2: (a): Transformation between the world (fixed), robot and sensor frames. The function T represents a homogeneous transformation. The transformation from robot frame to world frame is given by $T_{rw}(q_r)$, and the static transform from the sensor frame to robot frame is given by T_{sr} . For actuated touch sensors the sensor to robot frame transform is given by $T_{sr}(\psi)$ in which ψ represents the rotation of the sensor frame with respect to the robot frame. (b) Various configurations of compressible and (c) bendable touch sensor.

configuration is expressed by the variable $q_s = \delta$ and the robot state is the tuple $x = (q_r, \delta)$ in which $\delta \in [0, \delta_{max}]$ is the amount of compression along the sensor axis (as shown in Fig. 2b). For the bendable touch sensors (like Figs. 1b and 1e) we assume that the deflection from the nominal form is parameterized by $q_s = \alpha \in [\alpha_{min}, \alpha_{max}]$ in which $\alpha_{min} < 0 < \alpha_{max}$. If $\alpha = 0$ then the touch sensor is in its nominal form (see Fig. 2c). Thus, each α corresponds to a diffeomorphism that maps the points along the touch sensor at its nominal shape to the ones corresponding to $\alpha \neq 0$. The robot state x is the robot configuration and the sensor configuration, i.e., $x = (q_r, \alpha)$.

If the sensor can not change its configuration by itself but conforms to the environment, δ and α are not free variables. Consequently, their value can be derived from the robot configuration q_r and the environment description W , similar to closed kinematic chains. To this end, for each type of sensor, we can define a contact-constraint equation. For a compressible touch sensor,

$$\delta = f_{comp}(q_r, \partial W) \quad (3)$$

is the amount of compression for a given environment and robot configuration. Similarly,

$$\alpha = f_{bend}(q_r, \partial W) \quad (4)$$

describes the amount of deflection. The solution to Eq. (3) is unique, meaning that for each q_r we can uniquely determine the amount of compression. However, Eq. (4) can admit multiple solutions.

Finally, let $\mathcal{R}(x) \subset \mathbb{R}^2$ denote the points occupied by the robot in the world frame, equipped with the touch sensor at state x . The robot state space X is the set of all the states that the robot can be in without collisions. The robot is in collision if $\mathcal{R}(x) \cap W \neq \emptyset$.

C. Sensor models

We now introduce a family of touch sensors spanning rigid and compliant touch sensors. Although the discussion

focuses on a single unactuated touch sensor, the models presented herein can easily be extended to actuated touch sensors as will be discussed in Sec. III.

We first consider contact detectors such that the sensor is not compliant with the environment and it is fixed with respect to the robot (see, for example, Fig. 1a). The state in this case can be expressed solely by the robot configuration, i.e., $x = q_r$.

Model 1 (Contact detector): Let $p \in \mathbb{R}^2$ be the position of the contact detector whose coordinates are expressed in the sensor frame. The sensor mapping for the contact detector is

$$h_{cd}(x; p) = \begin{cases} 1 & \text{if } T_{rw}(q_r)T_{sr} \begin{pmatrix} p \\ 1 \end{pmatrix}^T \in \partial W \\ 0 & \text{otherwise.} \end{cases} \quad (5)$$

The preimages corresponding to h_{cd} result in a partition $\Pi(h_{cd})$ of two classes.

The next model describes a touch sensor when the contact can be detected along the touch sensor whose geometry is defined as the curve $\sigma : [0, 1] \rightarrow \mathbb{R}^2$ which maps to coordinates in the sensor frame.

Model 2 (Contact detector strip): Suppose there are N interior disjoint intervals, I_i , $i = 1, \dots, N$ such that $\bigcup_{i=1}^N I_i = [0, 1]$. Let the end points of N intervals correspond to a uniform discretization of $[0, 1]$ imposing a particular resolution. Let \mathcal{I} denote the set of N intervals and let \mathcal{I}_C be the set of intervals that are in contact with the boundary such that $\mathcal{I}_C = \{I \in \mathcal{I} \mid \exists p \in \sigma(I) \text{ s.t. } h_{cd}(x, p) = 1\} \subseteq \mathcal{I}$. Then, the contact detector strip is described by

$$h_{cds}(x, \sigma) = \mathcal{I}_C. \quad (6)$$

For the limiting case, as $N \rightarrow \infty$, the observation corresponds to the exact location (or locations) of contact along the strip. At the other extreme, when $N = 1$, the whole strip reduces to just one interval reporting whether a contact is made anywhere along the strip.

Next, we discuss a touch sensor that complies in response to touch by compressing along the sensor axis. The robot state is given by $x = (q_r, \delta)$ in which $\delta \in [0, \delta_{max}]$ is the amount of compression.

Model 3 (Compression sensor): The sensor which can detect the amount of compression in the touch sensor is described by

$$h_{cs}(x) = \delta. \quad (7)$$

The preimage of an observation $y = h_{cs}(x) > 0$ is typically a union of disjoint two-dimensional subsets of the state space. Suppose the length of the uncompressed touch sensor is ℓ . Let $P_\theta \subset W$ be the set of all points $u \in W$ for which there exists a $v \in \partial W$ such that a line segment \overline{uv} of length $\ell - \delta$ and slope θ satisfies $\overline{uv} \cap W = \emptyset$. Then $h_{cs}^{-1}(y) = \bigcup_{\theta \in S^1} P_\theta \times \{\theta\} \times \{y\}$. The preimage of $y = 0$ is all the states such that the touch sensor of length ℓ is not in collision. Thus, the states for which the touch sensor is in contact with the boundary and the ones such that the touch sensor lies completely in the interior of W belong to the same equivalence class and are indistinguishable.

Yet another form of compliance is the ability to bend under load. For this, consider the bendable touch sensors for which the state is $x = (q_r, \alpha)$.

Model 4 (Load sensor): This sensor can detect the amount of shear force applied to the compliant bendable touch sensor. This model addresses the transverse point load, a force applied at a single point along the touch sensor. The sensor mapping is described by

$$h_{ls}(x) = F, \quad (8)$$

and $F \in [-F_{max}, F_{max}]$, in which F_{max} is the maximum bearable load.

The next model describes the state of the robot in terms of $x = (q_r, \alpha)$, in which α is the deflection of the touch sensor upon contact. The load applied, physical dimension, and material property together determine the deflection.

Model 5 (Deflection sensor): The sensor which can detect the amount of deflection in the touch sensor is described by

$$h_{ds}(x) = \alpha. \quad (9)$$

For each $\alpha \in [\alpha_{min}, \alpha_{max}]$, the touch sensor has the shape described by the curve $\sigma_\alpha : [0, 1] \rightarrow \mathbb{R}^2$ which maps to the coordinates expressed in the sensor frame. The preimages for $y = h_{ds}(x) \neq 0$ is all states such that intersection of ∂W and the image of σ_α (coordinates mapped to the world frame) is not an empty set and that $\mathcal{R}(x) \setminus W = \emptyset$. This corresponds to a union of disjoint 2D or 3D (in case multiple orientations are possible to touch the boundary at some point along the sensor) subsets of the state space. Also for Model 5, for $y = 0$, the states for which the touch sensor is in contact with the boundary and the ones such that the touch sensor lies completely in the interior of W belong to the same equivalence class and are indistinguishable.

D. Composition of virtual touch sensors

Recall that the preimage corresponding to the observation $y = 0$ for Models 3 and 5 include also the states at which the sensor is not in contact with the environment which creates ambiguity. This can simply be alleviated by adding a contact detector at the touch sensor tip. To this end, Model 3 can be extended by combining it with Model 1 such that

$$h'_{cs}(q_r, \delta) = \begin{cases} \delta & \text{if } h_{cd}(q_r; p_t) = 1 \\ \# & \text{otherwise,} \end{cases} \quad (10)$$

in which $\#$ refers to no value and p_t is the point corresponding to the tip of the touch sensor whose exact location in sensor frame is $p_t = (\ell - \delta, 0)$. The same strategy can be followed also for bendable touch sensor corresponding to a deflection sensor (Model 5) in which case $p_t = \sigma_\alpha(1)$ and the respective sensor mapping is

$$h'_{ds}(q_r, \alpha) = \begin{cases} (\alpha, 1) & \text{if } h_{ds}(q_r; p_t) = 1 \\ (\alpha, 0) & \text{otherwise.} \end{cases} \quad (11)$$

On the other hand, the main issue with bendable touch sensors is the ambiguity regarding the point of contact. Unlike compressible touch sensors for which the contact

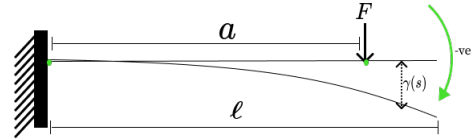


Fig. 3: A bendable touch sensor can be modeled as a simply supported cantilever beam of length ℓ . An intermediate load F is applied at a distance $a \leq \ell$ from the base in the positive direction of sensor axis. Then, $\gamma(s)$ is the deflection at any point s along the sensor such that $\gamma(0) = 0$ and maximum deflection is attained at ℓ .

needs to be at the tip to get a non-zero observation, bendable touch sensors can be in contact with the environment at any point along the sensor and still achieve that. To refine the preimages, we can enhance h_{ds} (Model 5) with a contact detector strip (Model 2). Suppose that the contact detector strip can conform to the shape assumed by the bendable touch sensor (like an elastic strip). The new sensor model is described as

$$h_{bc}(q_r, \alpha) = h_{cds}(q_r; \sigma_\alpha), \quad (12)$$

in which σ_α is the curve corresponding to the deflection determined by $\alpha = h_{ds}(x)$. The observation vector $y = h(x)$ would then correspond to the intervals (or points if $K = \infty$) such that the bendable touch sensor is in contact with ∂W . The partition of X resulting from the preimages of h , i.e., $\Pi(h_{bc})$, will be a refinement of $\Pi(h_{ds})$ such that each element of $\Pi(h_{bc})$ is a union of disjoint two-dimensional subsets of X .

Suppose the bendable sensor is in contact with the environment at a single point and let h_{bc} be the contact detector strip defined in Eq. (12) that reports the exact point of contact ($N = \infty$). Let $a = h_{bc}(x)$ be the point that is in contact with the boundary (coordinates expressed in the sensor frame), and let $F = h_{ls}(x)$ be the load acting on the sensor. If we consider only small deflections that satisfy the assumptions of classical beam theory, we can model the deflection from the nominal sensor shape as a function of the distance along the sensor length. Then, deflection $\gamma(s)$ (see Fig 3) at any $s \in [0, 1]$ under load $F = h_{ls}(x)$ can be calculated as [12]

$$\gamma(s) = \begin{cases} \frac{-F(s\ell)^2(3a-s\ell)}{6EI} & \text{if } 0 \leq s < \frac{a}{\ell} \\ \frac{-Fa^2(3s\ell-a)}{6EI} & \text{if } \frac{a}{\ell} \leq s < 1 \\ \frac{Fa^2(3\ell-a)}{6EI} & \text{if } s = 1, \end{cases} \quad (13)$$

in which E, I stand for the Young's modulus and moment of inertia, respectively, and ℓ is the sensor length. Note that the maximum deflection happens at the tip of the touch sensor. By considering small deflections, we also assume that the projection of the sensor tip on the horizontal axis of the sensor frame corresponds to ℓ and that the length of the sensor under load, that is, ℓ' satisfies $\ell' \approx \ell$. Consequently, we can define the curve corresponding to the bendable touch sensor as $\sigma_\alpha(s) = (s\ell, \gamma(s))$ in which $\alpha = h_{ds}(x)$. This provides an example when the composition of a load sensor

and a contact detector sensor in Eq. (12) is equivalent to a deflection sensor (Model 5).

III. COMPARISON TO VISIBILITY-BASED MODELS

In this section, we compare touch sensors from Sec. II-C with traditional depth sensors from [11] and evaluate conditions under which these are equivalent with respect to the definitions introduced in Sec. II-B.

A. Virtual depth sensors

Relevant depth sensor models are presented here for completeness. Let $Q = W \times S^1$ be the robot configuration space, that is, the set of all possible configurations of a point robot¹, over which a depth sensor is defined.

Model 6 (Depth-limited directional depth sensor): Let $b(q_r) \in \partial W$ denote the point struck by the ray emanating from (q_x, q_y) in the direction of q_θ . The sensor model is given by

$$h_{dds}(q_r) = \begin{cases} d(q_r) & \text{if } d_{min} \leq d(q_r) \leq d_{max} \\ \# & \text{otherwise,} \end{cases} \quad (14)$$

in which $d(q_r) = \|(q_x, q_y) - b(q_r)\|$ and $[d_{min}, d_{max}]$ with $d_{min} < d_{max}$ is the sensor detection range.

Suppose the depth-limited directional depth sensor (Model 6) is capable of emitting K evenly spaced rays, then such a sensor can observe $y = (y_1, \dots, y_k)$, simultaneously. Thus, we obtain a depth-limited K-directional depth sensor. The sensor mapping for such a sensor is then given by $h_{kdd}(q_r) = (y_1, \dots, y_K)$ in which $y_k = \|(q_x, q_y) - b(q_x, q_y, q_\theta + \phi_k)\|$ for every offset angle $\phi_k \in \{1, \dots, K\}$.

Model 7 (Depth-limited omnidirectional depth sensor): In the limit case, as $K \rightarrow \infty$, we obtain an omnidirectional depth sensor. In this case, the observation $h_{od}(q_r) = y$ is an entire function $y : [0, 2\pi) \rightarrow [d_{min}, d_{max}] \cup \{\#\}$ and

$$y(\phi) = h_{dds}(q_x, q_y, q_\theta + \phi). \quad (15)$$

B. Unactuated touch sensors

For compressible and bendable touch sensors, the state space X is a subset of the Cartesian product of the robot configuration space and possible touch sensor configurations. As the two families of sensors (depth sensors and touch sensors) do not share the same state space, they cannot be compared directly based on the previously introduced definitions of equivalence and sensor simulation. However, in the following, we will use a map from the state space to the robot configuration space to argue about these relations. Let $\text{proj} : X \rightarrow Q$ be a function that maps the state to its elements corresponding to the robot configuration. Consider a touch sensor h_1 and denote the partition induced by its preimages as $\Pi(h_1)$. Suppose proj is bijective. Then, the projection of the elements of each set in $\Pi(h_1)$ onto Q forms a partition of Q , denoted as $\Pi_Q(h_1)$. A touch sensor, h_1 , defined over X and a depth sensor, h_2 , defined over Q are

¹Note that we do not need to assume a point robot, and Q can as well be the set of all robot configurations such that the robot footprint is contained in W .

equivalent if the partitioning of the robot configuration space induced by the two sensors, $\Pi_Q(h_1)$ and $\Pi(h_2)$, respectively, satisfy $\Pi_Q(h_1) = \Pi(h_2)$. Similarly, h_1 can simulate h_2 if they are equivalent or if $\Pi_Q(h_1)$ is a refinement of $\Pi(h_2)$.

Since the contact constraint in Eq. (3) admits a unique solution, the mapping proj from the state space to robot configuration space is bijective for a compressible touch sensor, that is, there is a single state that the robot can be in for each robot configuration. Hence, if the compressible touch sensor is fully compressible, i.e., $\delta_{max} = \ell$, in which δ_{max} is the maximum attainable compression and ℓ is the sensor length, the projection of the elements in $\Pi(h_{cs})$ to Q forms a partition $\Pi_Q(h_{cs})$ of Q . Note that, if the touch sensor is not fully compressible, that is, $\delta_{max} < \ell$, then $\text{proj}(X) \subset Q$, meaning that there are some configurations that are not collision-free for a robot carrying a compressible touch sensor.

We now consider a fully compressible sensor of length ℓ together with a contact detector at the sensor tip, that is, h'_{cs} as given in Eq. (10), and a depth-limited directional depth sensor h_{dds} (Model 6) with $d_{min} = 0$ and $d_{max} = \ell$. The observation spaces Y_{cs} and Y_{dds} corresponding to h'_{cs} and h_{dds} are $Y_{cs} = Y_{dds} = [0, \ell]$. Suppose the touch sensor frame is aligned with the robot frame such that $\psi = 0$ and $T_{sr}(\psi)$ is the identity matrix (see Fig. 2). Then, we can define a function $g : Y_{cs} \rightarrow Y_{dds}$ such that $h_{dds}(q_r) = (g \circ h_{cs})(q_r, \delta) = \ell - h_{cs}(q_r, \delta)$ which implies that $\Pi_Q(h'_{cs}) = \Pi(h_{dds})$ and proves that the following proposition holds.

Proposition 1: A fully compressible touch sensor h'_{cs} of length ℓ as described in Eq. (10) can simulate (in the sense from Section II-A) a depth-limited directional depth sensor with $d_{min} = 0$ and $d_{max} = \ell$.

For the limiting case, as $\ell \rightarrow \infty$, a fully retractable compression sensor of length ℓ can simulate a directional depth sensor ($d_{max} = \infty$), which returns the distance to the closest point on the environment boundary along the direction of q_θ . At the other extreme, for $\ell = 0$, h_{cs} is merely a contact detector h_{cd} (Model 1) with $p = (0, 0)$. Furthermore, it follows from Proposition 1 that an array of K fully compressible touch sensors with length ℓ , arranged at angles ψ_1, \dots, ψ_K with respect to the robot reference frame such that simultaneous observations yield the vector (y_1, \dots, y_K) can simulate a depth-limited K-directional depth sensor h_{kdd} described in Sec. III-A.

For a bendable touch sensor, the solution to contact constraint in Eq. (4) may not be unique. For instance, consider the scenario as shown in Fig. 4 in which touch sensor it can be in multiple deflection modes (corresponding to different α) at the same configuration $q_r = (q_x, q_y, q_\theta)$. Thus, proj is a many to one mapping and the projection of the elements of $\Pi(h_{ds})$ to Q corresponds to a cover of Q . This implies that we can not compare h_{ds} with another sensor defined over Q in terms of previously introduced definitions of equivalence and sensor simulation.

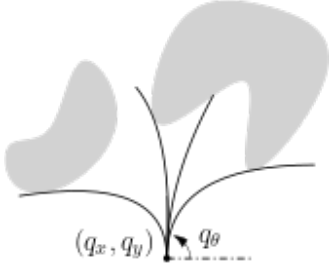


Fig. 4: A bendable touch sensor can be in multiple different modes at the same robot configuration. Therefore, the solution to the contact constraint is not unique.

C. Actuated touch sensors

Suppose that the touch sensor is attached to a revolute joint that can be controlled to change its configuration. The state of the system x now includes the robot configuration q_r and the joint configuration $\psi \in S^1$ such that $x = (q_r, \psi, \dots)$. A measurement is obtained by changing the configuration of the revolute joint while the robot configuration q_r is kept constant. Let a state trajectory up to time t be denoted as $\tilde{x} : [0, t] \rightarrow X$. The set of all state-trajectories such that $\text{proj}(x)$ is constant for all $x \in \tilde{x}$ for any possible $t > 0$ is denoted by \tilde{X} . The sensor mapping for an actuated sensor is $h : \tilde{X} \rightarrow Y$. Since the state is now augmented with the joint configuration, in the following, with a slight abuse of previously introduced definitions, we consider the sensor models in Section II-C to be defined over this extended state space.

We begin by considering a compressible touch sensor described as h'_{cs} in Eq. 10 attached to a revolute joint. The state of the system is expressed by $x = (q_r, \psi, \delta)$. Suppose that for each measurement, the revolute joint trajectory corresponds to a full rotation of the sensor that is defined as $\tilde{\psi} : [0, t] \rightarrow S^1$ such that $\tilde{\psi}$ is a monotonically increasing function with $\tilde{\psi}(0) = 0$ and $\tilde{\psi}(t) = 2\pi$ while $\text{proj}(\tilde{x}(\tau)) = q_r, \forall \tau \in [0, t]$.

Let $\tilde{X}_{fr} \subseteq \tilde{X}$ be the set of all trajectories that satisfy this motion. It follows from Proposition 1 that h'_{cs} can be used to obtain the distance to the boundary (up to ℓ) along the sensor axis, which corresponds to the direction of $q_\theta + \psi$ for an actuated touch sensor. Then, $\forall \psi \in [0, 2\pi)$ the shifted distance $d(q_x, q_y, q_\theta + \psi) = \ell - h'_{cs}(x)$. Considering the full motion that spans all $\psi \in [0, 2\pi)$, h'_{cs} combined with motion results in the observation $y : S^1 \rightarrow [0, \ell]$ such that $y(\psi) = d(q_x, q_y, q_\theta + \psi)$ if $d(q_x, q_y, q_\theta + \psi) \leq \ell$ and $y(\psi) = \#$, otherwise. Then, the following proposition holds.

Proposition 2: Suppose \tilde{X}_{fr} corresponding to the full rotation of the revolute joint is not empty. Let $Q' \subseteq Q$ be defined as $Q' = \bigcup_{\tilde{x} \in \tilde{X}_{fr}} \text{proj}(\tilde{x}(0))$. Then, an actuated compressible sensor as defined above can simulate (in the sense from Section II-A) a depth-limited omnidirectional depth sensor (Model 7) defined over Q' .

The main reason why an actuated compressible touch sensor (even if it is fully compressible) may not simulate a depth-limited omnidirectional depth sensor defined over the

entire Q is that for certain q_r a full rotation of the revolute joint may not be possible due to the sensor characteristics and the environment (see for example, Fig. 6). This issue could be alleviated to some extent (although not fully) by defining a slightly more complicated motion (for example, a full (or partial) counterclockwise (ccw) followed by a rotation in the clockwise (cw) direction) or with the sensor design. To this end, configuration space decomposition of a robot carrying a compressible sensor and determining its connectivity remains as an interesting open problem.

We now consider a mobile robot equipped with a bendable touch sensor composed of a bendable link together with a deflection sensor (Model 5) attached to a revolute joint. The state of the system is expressed as $x = (q_r, \psi, \alpha)$. Considering the same motion corresponding to a full rotation of the revolute joint, let $P \subset W$ be part of the environment swept by the touch sensor such that

$$P = \bigcup_{x \in \tilde{x}} \bigcup_{s \in [0, 1]} T_{rw}(q_r) T_{sr}(\psi) \sigma_\alpha(s). \quad (16)$$

The observation is the function $y(\psi) = h_{ds}(x)$. The preimage of y contains all possible robot configurations q_r such that same profile information is obtained, i.e., all q_r such that $P \in W$ and $\partial P \cap \partial W \neq \emptyset$, in which ∂P is the boundary of the area swept by the touch sensor. Note that the preimages corresponding to the combination of rotary motion and deflection sensor still result in a cover of the robot configuration space since different P can be obtained for the same q_r based on the configuration of the bendable touch sensor at the beginning of the motion.

We now consider a motion similar to actuated whisking (see for example [10], [13]) which corresponds to a full ccw rotation followed by a full cw rotation. In the following, we will show that with this type of motion, under certain conditions, a bendable touch sensor with a deflection sensor can simulate a depth sensor. Let $\mathcal{D}_\ell(q_x, q_y)$ denote the disk of radius ℓ centered at (q_x, q_y) as shown in Fig. 5. Suppose that $\mathcal{D}_\ell(q_x, q_y) \setminus W$ (light gray area in Fig. 5) is convex and that at the beginning of the motion, the touch sensor is in its nominal form, that is, $\alpha = 0$. Denote the intersection point of the touch sensor at the beginning of the motion and the boundary of $\mathcal{D}_\ell(q_x, q_y)$ as p_0 . The instances at which α changes from zero to non-zero or non-zero to zero are called critical instances and they happen when the touch sensor starts bending or regains its nominal form. Since $\mathcal{D}_\ell(q_x, q_y) \setminus W$ is convex, a rotation in single direction results in at most two critical instances: when the sensor gets in contact with the boundary of W so it starts bending and if possible, when it regains its nominal shape. Suppose, during a full rotation in the ccw direction, the nominal shape is achieved after bending and the swept area is denoted by P_{ccw} . Let $p_1, p_2 \in \partial \mathcal{D}_\ell(q_x, q_y)$ be the intersection points of the touch sensor and $\partial \mathcal{D}_\ell(q_x, q_y)$ at the beginning and at the end of the bending, respectively (see Fig. 5). We assume that $P_{ccw} \cap \partial W$ is a connected curve. Let u_1 be an endpoint of this curve which corresponds to the last point along the ∂W that the touch sensor is in contact with during a ccw

motion. For cw rotation, denote the swept area by P_{cw} and define p_3, p_4 , similar to p_1, p_2 , and define u_2 similar to u_1 . We again assume that $P_{cw} \cap \partial W$ is connected. We say that p' lies to the left of p if p' lies on the left hand side of the ray starting at (q_x, q_y) and passing through p , the relation is denoted by $p' >_\ell p$.

Let $V(q_x, q_y) \subseteq W$ be the set of points visible from (q_x, q_y) . A point $p' \in W$ is visible from $p \in W$ if the line segment $\overline{pp'}$ is contained in W . The following lemma establishes a relation between the visibility of (q_x, q_y) and a bendable sensor at (q_x, q_y) executing a whisking motion as described above which satisfies the assumptions.

Lemma 1: Suppose $\mathcal{D}_\ell(q_x, q_y) \setminus W$ is convex, and suppose that $u_1 >_\ell u_2$ and $p_0 >_\ell p_2$. Then, $P = \mathcal{D}_\ell(q_x, q_y) \cap V(q_x, q_y)$, in which $P = P_{ccw} \cup P_{cw}$.

Proof: Since $\mathcal{D}_\ell(q_x, q_y) \setminus W$ is convex, there are two tangents from (q_x, q_y) . Let \vec{r}_r and \vec{r}_ℓ be two rays starting from (q_x, q_y) and representing the right and left tangents, respectively (see Fig. 5). Rays \vec{r}_r and \vec{r}_ℓ intersect the boundary of $\mathcal{D}_\ell(q_x, q_y)$ at two distinct points, denoted by p_r and p_ℓ , respectively. Let $p_\ell \hat{\ } p_r$ be the circular arc from p_ℓ to p_r . A circular arc $p \hat{\ } p'$ satisfies $p'' >_\ell p, \forall p'' \in p \hat{\ } p'$. Let A (green area in Fig. 5) be the circular sector corresponding to the arc $p_\ell \hat{\ } p_r$ and let B (blue area in Fig. 5) be the connected region bounded by \vec{r}_r (corresponding to the left half-plane determined by \vec{r}_r), \vec{r}_ℓ (corresponding to the right half-plane determined by \vec{r}_ℓ) and ∂W that includes (q_x, q_y) . Then, $\mathcal{D}_\ell(q_x, q_y) \cap V(q_x, q_y) = A \cup B$. Consider the ccw motion. The area swept before bending is the circular sector determined by the arc $p_0 \hat{\ } p_1$. Since $p_0 >_\ell p_2$, sensor achieves its nominal form before it reaches back to p_0 . Then, the total area swept with $\alpha = 0$ is the circular sector determined by $p_0 \hat{\ } p_1$. Furthermore, since p_1 is the intersection point when the bending begins, the ray starting at (q_x, q_y) and passing through p_1 is the right tangent \vec{r}_r . Similarly, consider the cw motion. The area swept before the bending begins is the circular sector determined by the arc $p_3 \hat{\ } p_0$. Since p_3 is before the sensor begins to bend, the ray starting at (q_x, q_y) and passing through p_3 corresponds the left tangent \vec{r}_ℓ . Hence, $p_3 = p_\ell$. Consequently, the union of the two circular sectors corresponding to area swept with $\alpha = 0$ resulting from ccw and cw motion equals to A . Since $P_{cw} \cap \partial W$ and $P_{ccw} \cap \partial W$ are two connected curves and $u_1 >_\ell u_2$, part of ∂W visible from (q_x, q_y) is swept. Furthermore, bending is a continuous deformation which implies that the swept area does not have any holes. Then, the area swept for $\alpha \neq 0$ equals to B . This shows that $A \cup B = \mathcal{D}_\ell(q_x, q_y) \cap V(q_x, q_y) = P$, in which $P = P_{cw} \cup P_{ccw}$. \square

Let \tilde{X}_w be the set of all trajectories corresponding to the whisking motion and let $\tilde{X}'_w \subseteq \tilde{X}_w$ be the ones such that for each $\tilde{x} \in \tilde{X}'_w$ it is true for the corresponding swept area P that $u_1 >_\ell u_2$ and $p_0 >_\ell p_2$ and that $\mathcal{D}_\ell(q_x, q_y) \setminus W$ with respect to the robot configuration $\text{proj}(\tilde{x}(0)) = q_r$ is convex. We can now compare a bendable touch sensor with a depth sensor owing to the inclusion of motion.

Proposition 3: Suppose \tilde{X}'_w is not empty. Let $Q' \subseteq Q$

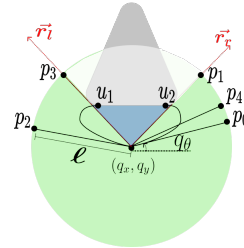


Fig. 5: Critical points for an actuated bendable touch sensor mounted on a revolute joint capable of cw and ccw motions. Light gray area corresponds to $\mathcal{D}_\ell(q_x, q_y) \setminus W$, green area is A and blue area is B .

be defined as $Q' = \bigcup_{\tilde{x} \in \tilde{X}'_w} \text{proj}(\tilde{x}(0))$. Then, an actuated deflection touch sensor with a contact detector at the tip executing a whisking motion as defined above can simulate (in the sense from Section II-A) h_{od} (Model 7) defined over Q' .

Proof: It follows from Lemma 1 that for each $q_r \in Q'$, the swept area P with respect to the trajectory $\tilde{x} \in \tilde{X}'_w$ such that $\text{proj}(\tilde{x}(0)) = q_r$ satisfies $P = \mathcal{D}_\ell(q_x, q_y) \cap V(q_x, q_y)$. Then we can define function $y : [0, 2\pi) \rightarrow [0, \ell]$ such that $y(\psi) = \|(q_x, q_y) - b_P(q_x, q_y, q_\theta + \psi)\|$, in which $b_P(q_x, q_y, q_\theta + \psi)$ is the point struck on the boundary of ∂P by the ray in the direction of $q_\theta + \psi$ starting from (q_x, q_y) if no $x = (q_x, q_y, q_\theta, \psi, \alpha) \in \tilde{x}$ satisfies $h'_{ds}(x) = (0, 0)$ (see Eq. (11) and recall that all the sensor mappings are now defined over the augmented state space), and $\#$ otherwise. Finally P is defined as Eq. (16) for a whisking motion using h'_{ds} (Model 5) to determine σ_α for each $x \in \tilde{x}$. \square

Similar to rotary motion, one can consider a translational motion too, in which case the touch sensor is swept (if in contact) along the boundary of the environment. This introduces an additional complexity since the robot configuration is no longer fixed over the course of sensor movement. We expect translational motion together with a rotational motion (similar to whisking) to be the most useful for touch based navigation. However, we will investigate such touch behaviors in future works.

IV. DISCUSSION

In this work, we introduced several *virtual touch sensor models* of a touch sensor mounted on a mobile robot. Although some of these models were abstract in nature, others were shown to be equivalent to conventional visibility-based models. The motivation behind this study was to elevate the scattered use of touch sensors up to the level of a broad sensor category that warrants systematic modeling to better understand their applications for navigation. This would then inspire designing more navigation centric touch sensors which could be mounted on a mobile robot for safely exploring unknown environments. This is especially useful in vision devoid scenarios like underwater inspections in murky waters or exploration in areas with suspended caustic chemicals that would otherwise damage sensors like

cameras and Lidars. Mobile robots endowed with touch sensing abilities and deployed in unstructured environments can benefit from our study in various domains such as health care, sports, ergonomics, industry, distribution of goods, and service robotics.

Existing touch sensor designs are primarily geared towards furthering our understanding of touch receptors such as vibrissae in rats [14] and human-like grasping [15]. However, touch sensors such as the contact strip (Model 2) and the compression sensor (Model 3) are also useful in reducing the uncertainty in state estimate while ensuring the safety of the touch sensor and the robot.

When comparing *virtual sensor models*, the main difficulty was the lack of shared state space across various sensors under consideration (as certain configurations are not feasible for touch sensors). This can be alleviated by designing touch sensors which are fully compressible, retractable, and/or bendable. To illustrate, consider the scenario shown in Fig. 6 where the touch sensor disrupts the connectivity of the robot configuration space. In such cases, using a different touch sensor (such as a bendable touch sensor) can be the solution. Additionally, for real world deployment, touch sensors need to be robust to wear and tear and the abilities such as telescopic extensions or fully retractable compression can help the robot maneuver even in tight spaces by modulating its footprint which is otherwise not feasible when using conventional sensors like a camera.

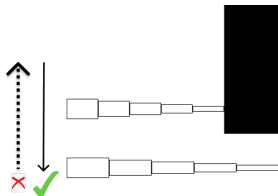


Fig. 6: Navigation limitations with compression sensor

The next step in our study would be to consider actuated touch sensors on a mobile base such that the system would have both rotational and translation degrees of freedom as opposed to only rotation as considered above. This would open new avenues for developing impact-resilient robots by utilizing touch sensor feedback-based motion primitives. The models presented here were for an ideal touch sensor however, the abstract models independent of their physical realization could very well serve a purpose similar to the pinhole camera model for computer vision. For the real world, sensor noise needs to be accounted for. To address the stochastic nature of the sensors, sensor fusion and effective data representation algorithms are critical aspects to consider when using touch sensors for mobile robot navigation. Sensor fusion techniques could be used for combining spatial, temporal, or spatiotemporal sensor data from multiple modules of the same sensor (as in a vibrissal array) or heterogeneous sensors (as in fusing touch sensor data with other on board sensors). As a result, developing efficient filtering and sensor fusion algorithms for processing touch data becomes a prior-

ity, especially tactile SLAM. Recent attempts at sensor fusion (see [16], [17]) show promising performance improvements when touch sensor information is fused with other sensors on board such as cameras which have longer detection range and dense area coverage. Touch sensors, despite their short range, can complement such sensors and dedicated filters for fusing information need to be developed. Aside from accounting for noise, the ideal models considered in this work can also be extended to more practical situations such as those involving multiple forces simultaneously acting on the cantilever, and simultaneous compression and deflecting of the beam.

REFERENCES

- [1] R. A. Grant, A. L. Sperber, and T. J. Prescott, "The role of orienting in vibrissal touch sensing," *Frontiers in behavioral neuroscience*, vol. 6, p. 39, 2012.
- [2] G. Reina, L. Ojeda, A. Milella, and J. Borenstein, "Wheel slippage and sinkage detection for planetary rovers," *IEEE/Asme Transactions on Mechatronics*, vol. 11, no. 2, pp. 185–195, 2006.
- [3] G. M. Hegde, C. Ye, C. A. Robinson, A. Stroupe, and E. Tunstel, "Computer-vision-based wheel sinkage estimation for robot navigation on lunar terrain," *IEEE/ASME Transactions on Mechatronics*, vol. 18, no. 4, pp. 1346–1356, 2013.
- [4] G. R. Scholz and C. D. Rahn, "Profile sensing with an actuated whisker," *IEEE Transactions on Robotics and Automation*, vol. 20, no. 1, pp. 124–127, 2004.
- [5] J. An, P. Chen, Z. Wang, A. Berbille, H. Pang, Y. Jiang, T. Jiang, and Z. L. Wang, "Biomimetic hairy whiskers for robotic skin tactility," *Advanced Materials*, p. 2101891, 2021.
- [6] D. I. McCloskey, "Kinesthesia, kinesthetic perception," in *Sensory Systems: II*. Springer, 1988, pp. 36–38.
- [7] J. C. Tuthill and E. Azim, "Proprioception," *Current Biology*, vol. 28, no. 5, pp. R194–R203, 2018.
- [8] Z. Lu, Z. Liu, and K. Karydis, "Deformation recovery control and post-impact trajectory replanning for collision-resilient mobile robots," in *2021 IEEE/RSJ International Conference on Intelligent Robots and Systems (IROS)*. IEEE, 2021, pp. 2030–2037.
- [9] P. Giguere and G. Dudek, "A simple tactile probe for surface identification by mobile robots," *IEEE Transactions on Robotics*, vol. 27, no. 3, pp. 534–544, 2011.
- [10] N. F. Lepora, M. Pearson, and L. Cramphorn, "Tacwhiskers: Biomimetic optical tactile whiskered robots," in *2018 IEEE/RSJ International Conference on Intelligent Robots and Systems (IROS)*. IEEE, 2018, pp. 7628–7634.
- [11] S. M. LaValle, *Sensing and filtering: A fresh perspective based on preimages and information spaces*. Now Publishers, 2012.
- [12] J. E. Shigley, *Shigley's mechanical engineering design*. Tata McGraw-Hill Education, 2011, ch. 4.
- [13] T. J. Prescott, M. J. Pearson, B. Mitchinson, J. C. W. Sullivan, and A. G. Pipe, "Whisking with robots," *IEEE robotics & automation magazine*, vol. 16, no. 3, pp. 42–50, 2009.
- [14] M. J. Pearson, B. Mitchinson, J. C. Sullivan, A. G. Pipe, and T. J. Prescott, "Biomimetic vibrissal sensing for robots," *Philosophical Transactions of the Royal Society B: Biological Sciences*, vol. 366, no. 1581, pp. 3085–3096, 2011.
- [15] W. Chen, H. Khamis, I. Birznieks, N. F. Lepora, and S. J. Redmond, "Tactile sensors for friction estimation and incipient slip detection—toward dexterous robotic manipulation: A review," *IEEE Sensors Journal*, vol. 18, no. 22, pp. 9049–9064, 2018.
- [16] O. Struckmeier, K. Tiwari, M. Salman, M. J. Pearson, and V. Kyrki, "ViTa-SLAM: A bio-inspired visuo-tactile slam for navigation while interacting with aliased environments," in *2019 IEEE International Conference on Cyborg and Bionic Systems (CBS)*. IEEE, 2019, pp. 97–103.
- [17] M. J. Pearson, S. Dora, O. Struckmeier, T. C. Knowles, B. Mitchinson, K. Tiwari, V. Kyrki, S. Bohte, and C. M. Pennartz, "Multimodal representation learning for place recognition using deep Hebbian predictive coding," *Frontiers in Robotics and AI*, vol. 8, 2021.